Response of coaxial air-assisted liquid jets in an acoustic field: atomization and droplets clustering

A. Ficuciello, J. Blaisot, F. Baillot, C. Richard, M. Theron

Response of coaxial air-assisted liquid jets in an acoustic field: atomization and droplets clustering

A. Ficuciello[1,3], J.B. Blaisot[1], F. Baillot[1], C. Richard[2] and M. Théron[3]

[1]CORIA, UMR 6614, CNRS Université et INSA de ROUEN, BP 12,76801 Saint Etienne du Rouvray, France
[2]LMRS, UMR 6085, CNRS-Université de ROUEN, BP 12,76801 Saint Etienne du Rouvray, France
[3]CNES Launchers Directorate, 52 rue Jacques Hillairet, 75612 PARIS Cedex, France

Abstract

High-frequency combustion instabilities have been proven to be extremely harmful to liquid rocket engine operation, even leading to the destruction of the combustion chamber. The coupling between acoustic field and combustion heat release rate in the combustion chamber is considered as the driving phenomenon. Experiments have shown that intense acoustic field can deeply affect atomization process thereby causing a non-uniform heat release distribution which can couple with the resonant mode shapes of the combustion chamber and consequently trigger or sustain combustion instability.
The effects of acoustic acting on atomization of coaxial air-assisted liquid jets have been investigated experimentally and results are presented in this paper.
The experimental set-up is composed of three coaxial injectors installed on the roof of a semi-open resonant cavity provided with 4 compression drivers. An acoustic field corresponding to the 2nd transverse mode of the cavity is forced into that at a frequency of 1 kHz. Acoustic levels up to 174 dB are produced. High speed visualizations are performed in order to observe the response of the jet to the acoustic perturbations.
In the case of low Weber numbers (We < 30) the jet can be considered as cylindrical and depending on the position of the injector with respect to the acoustic axis different responses can be observed. If the injector is placed in correspondence of the velocity antinode the jet is flattened into a liquid sheet perpendicular to the acoustic axis, if the injector is located in correspondence of an intensity antinode the jet is deviated toward the velocity antinode. Combined response can be observed at intermediate positions.
For higher Weber numbers the jet is no more cylindrical and a spray is formed, characterized by with a certain spray angle. Such a spray is can still be affected by the acoustics but it is not always possible to get evidence of this from observation of raw images. To quantify these effects, image analyses have been carried-out to determine how spatial distributions of droplets are affected by acoustics.
Results are presented for Weber numbers ranging from 30 to 1500, with and without acoustic. Clustering of droplets is shown as well as improvement of atomization process.

Keywords: Atomization, acoustics, combustion instability, liquid rocket engine

Introduction

Since the early development of liquid rocket engines in the 1940s, combustion instabilities represented one of the biggest issues limiting propulsion system reliability. High frequency transversal combustion instabilities are considered to be the most destructive [1]. This kind of phenomenon is common in rocket combustors due to the high energy release rate. Typically, since liquid rocket combustor can be seen as a nearly closed cavity, damping is minimized and small perturbations can grow to destructive amplitudes very quickly.

Combustion instabilities are rarely discussed without referring to the Rayleigh criterion, which states that heat release must be in phase with the pressure oscillation in order to allow resonant interaction between combustion and acoustic field. Moreover, as the coupling mechanism can be driven by pressure or velocity, not only the phase between pressure and heat release has to be considered but also the characteristic spatial distribution of the acoustic pressure and velocity field. Sliphorst et al. [2] observed that if the velocity anti-node is in the combustion zone, most energy is transferred into the acoustic field, indicating velocity as the driver mechanism. Such a phenomenon could be explained by admitting an improvement of the atomization process in correspondence of the velocity anti-node causing a local increase of the heat release. Another work dedicated to the study of the dynamics of cryogenic flames under effects of acoustic field showed that flame length and atomization process are modified by the acoustics, and in some conditions an asymmetry in the flame distribution is observed [3]. It is thus clear that among the multiple processes involved, atomization could play an important role in driving

instability. In fact, previous researches have pointed out how acoustic field with sufficiently high amplitude can drastically affect the behaviour of an air-assisted coaxial jet [4][5][6]. In these works the response of jets to the acoustic field in correspondence of the velocity and intensity anti-node has been ascribed to non-linear acoustic effects, involving the local radiation pressure distribution and the resulting radiation pressure force. In particular, flattening of the jet was observed in correspondence of the velocity anti-node, and a deviation from the vertical axis in correspondence of the intensity anti-node. It was also concluded that the higher the Weber number of the air-assisted jet, the higher the acoustic pressure level threshold was needed.
In the present study additional intermediate locations with respect to the acoustic axis are taken into account. Atomization regimes at high Weber number will be considered in order to approach to liquid rocket engine propellant injection operative conditions and it will be shown as acoustics influence the behaviour of the jet, in a way similar to what observed in hot fire tests previously cited.

Experimental set-up and procedure

The experimental set-up is composed of an acoustic semi-opened resonant cavity which consists of two parallel and vertical steel plates and PVC roof and floor. A pair of compression drivers Beyma CP850Nd is placed on each vertical plate. The acoustic field can be identified, at first approximation, as the 2nd transverse mode of the cavity (see Figure 1).

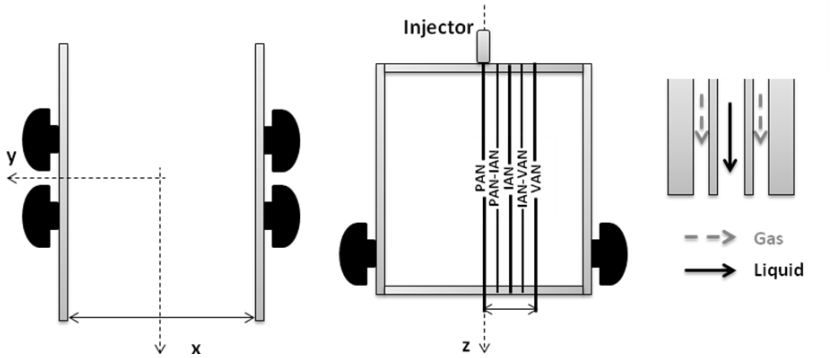

Figure 1 Experimental test-rig: (a) upper-side view of the acoustic cavity, (b) front-side view of the cavity and characteristic acoustic reference locations, (c) injector sketch.

The maximum acoustic pressure, reached on the top centre of the cavity (pressure anti-node), is 174 dB and two acoustic pressure minima are detected in correspondence of the two velocity anti-nodes. A coaxial injector with a central orifice for the liquid flow and an external annulus for the gas flow is placed in the acoustic cavity such that its exit plane coincides with the inner surface of the roof. The liquid used is water, and the gas flowing around the liquid jet is air. Up to three injectors can be simultaneously placed on the roof, but results discussed in the following are performed with only one injector.

Five different locations along the acoustic axis are investigated i.e. the pressure anti-node (PAN), the intensity anti-node (IAN), the velocity anti-node (VAN) and the positions between the pressure anti-node and the intensity anti-node (PAN-IAN) and between the intensity anti-node and the velocity antinode (IAN-VAN).

For each location several flow conditions have been investigated in order to cover all atomization regimes, as identified by Lasheras & Hoppfinger [7]. The response to the acoustic perturbation of the two phase flow from low Weber number corresponding to Rayleigh axi-symmetric regime ($We < 30$, $Re_L \sim 2000$) to high Weber number, corresponding to the membrane and fiber regimes ($100 < We < 1500$, $Re_L \sim 4000$) are considered here. High speed visualizations were performed with a Vision Research Phantom V12 camera at 6273 fps. A white continuous light source (Lot-Oriel LSB530, 300W) is used in this case with a diffuser plate.

The acoustic perturbation provided by the 4 loudspeakers is generated with an amplitude envelop comprising first a ramp from 0 to Pac^{max}, a constant part at Pac^{max} and a decreasing ramp from Pac^{max} to 0 at the end of signal generation. Each part lasts 300 ms. Image are recorded during total length of acoustic signal duration that corresponds to a sequence of 8216 frames. The image analysis is performed on image sub-sequences extracted from complete sequences. The first 200 frames (t = 0.03188 s) correspond to the beginning of the ramp, is referred as ITi, the sequence of 200 frames extracted during the maximum amplitude period of the acoustic field is referred as ITac. Another treatment has been performed on 200 frames of high speed visualization without acoustics, referred as IT0.

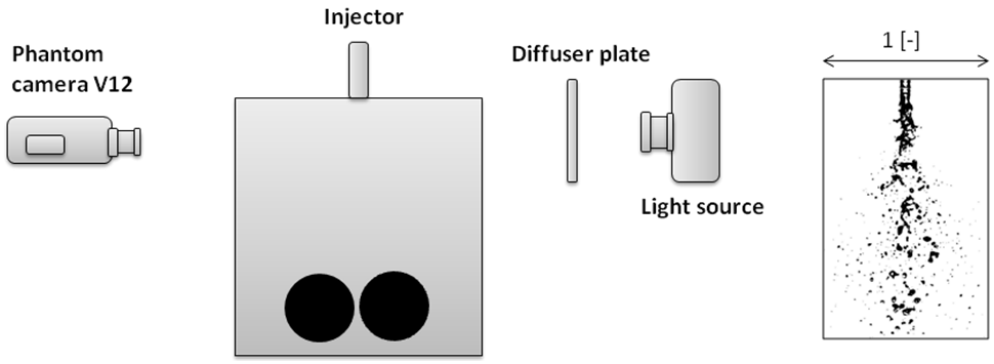

Figure 2 (a) Experimental mounting for high-speed visualization, (b) typical example of output image with normalized width.

Comparison between ITi and IT0 has shown that even if the number of frames considered in ITi represents 1/10 of the overall ramp some acoustic effects are already visible. Those effects are anyway negligible with respect to the dramatic response of the jet during maximum acoustic solicitation. Image treatment has been performed with several home-made softwares [8]. Concerning the dispersed phase a morphological criterion was applied in order to consider spherical or pseudo-spherical elements.

Results and Discussion

In the case of jets at low Weber number such as the Rayleigh axi-symmetric regime, the jet can be considered at first approximation as cylindrical. Its response to the acoustic perturbation can be explained by taking into account acoustics non-linear effects, in particular considering the distribution around the jet of the radiation pressure p_{rad} [9][10]. When the injector is placed in correspondence of the velocity anti-node (VAN) the distribution of p_{rad} is not uniform around the jet, causing a suction effect in one direction and consequently the jet is flattened perpendicularly to the acoustic axis. A liquid sheet is thus formed, which successively brakes-up under the effects of Faraday's instability producing an intense spray.

Moving away from the velocity anti-node the distribution of the radiation pressure starts to be non symmetric with respect to the acoustic axis. As result, integration of p_{rad} along the cylinder circumference is not null and it results in a force, named radiation force that cause the deviation of the jet toward the nearest velocity antinode. The radiation force presents is maximum in correspondence of the intensity antinode (IAN) [4] but the maximum deviation angle is observed in between this position and the pressure antinode (PAN). In fact, at IAN there is still a flattening effect which causes a deformation of the jet and promote atomization.

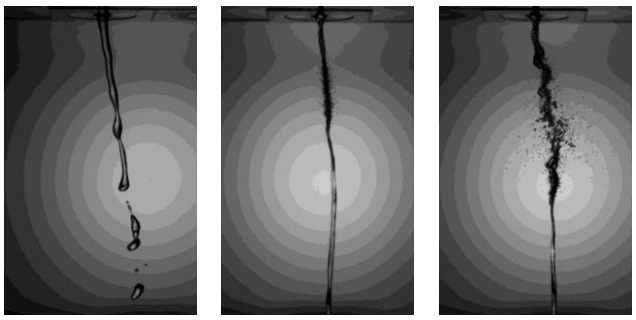

Figure 3 Acoustics effects on Rayleigh axi-symmetric jets at:
(a) PAN-IAN, (b) IAN and (c) IAN-VAN.

Between IAN and PAN almost no flattening is observed and the jet is deviated with a constant angle all along the jet length (see Figure 3). No effects are observed at the pressure anti-node where distribution of p_{rad} around the jet is uniform.

Increasing the Weber number the jet cannot be considered as cylindrical anymore because a spray is formed without acoustics, but responses similar to the ones provided by the Rayleigh axi-symmetric regime can be observed. In fact, in correspondence of VAN an increase in the average number of droplets is observed. For a jet in

the membrane regime (We = 100) the number of drops during acoustics is around ten times the one without acoustics while for the fiber regime (We = 220) droplets number increases only of a factor 2. The difference between these two values can be explained by considering that the liquid blobs present in the membrane regime can be broken up by acoustics into smaller droplets more easily than the small liquid objects present in the fiber regime. If the injector is placed between the intensity anti-node and the velocity anti-node no variation in the droplets number is observed for the fiber regime while a ratio around 8 is obtained for the jet in the membrane regime. At IAN and between IAN and PAN this ratio is around 2 for the membrane regime and still close to the unity for the fiber case.

The effects of the acoustics in terms of atomization improvement are stronger in correspondence of VAN and less and less visible going toward the PAN and as already observed for the Rayleigh axi-symmetric regime droplets are deviated toward the nearest velocity antinode.

Figure 4 shows the horizontal normalized probability density function of droplet position $\mathrm{Pdf}_i(\tilde{y})$ for the 5 locations considered along the acoustic axis as presented before. For each class the number of objects all over the 200 frames is counted in, and it is normalized by the sum of the elements of all classes times the width of the class adimensionalized by the image width (w_i). Thus the non-dimensional horizontal position is $\tilde{y} = y/w_i$.

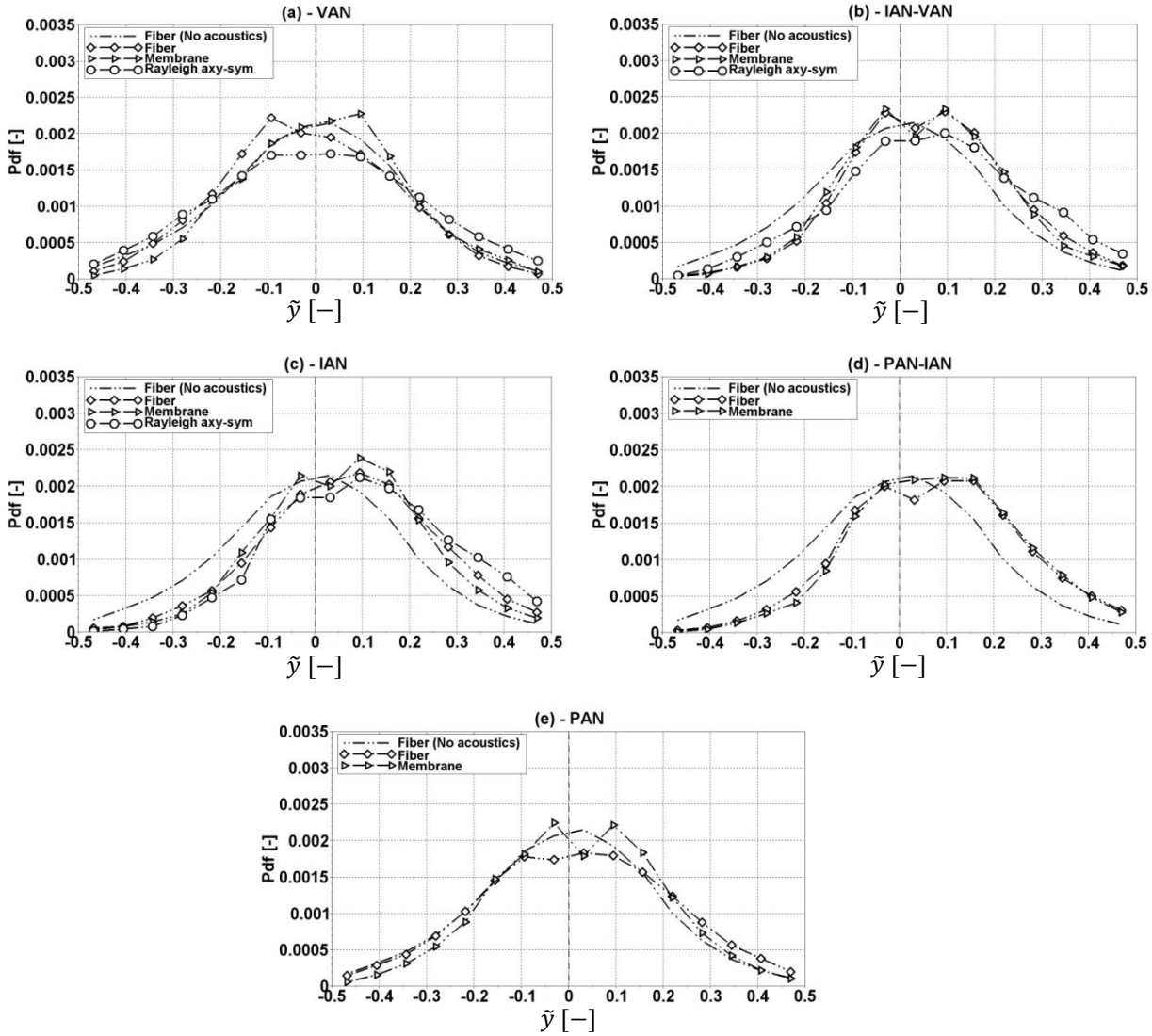

Figure 4 Pdf for the fiber, membrane and Rayleigh regime during maximum acoustics perturbation compared with the Pdf in the case of the fiber regime without acoustics.

The Pdf for the three regimes discussed before (Rayleigh, membrane and fiber) during maximum acoustic perturbation (ITac) are compared along with the Pdf of the fiber regime without acoustics (IT0). In correspondence of VAN (Figure 4a) and PAN (Figure 4e) the distributions with acoustics are symmetrical with respect to the central axis (axis of the injector) while for IAN-VAN location (Figure 4b) an accumulation of droplets on the

right side of the images is observed, that is even more pronounced in the case of IAN (Figure 4c) and between IAN and PAN (Figure 4d). In each one of the five locations considered, Pdf are similar no matter what is the initial state. Even if without acoustics, Rayleigh and fiber regime are completely different, once acoustics is turned on the same effects can be observed.

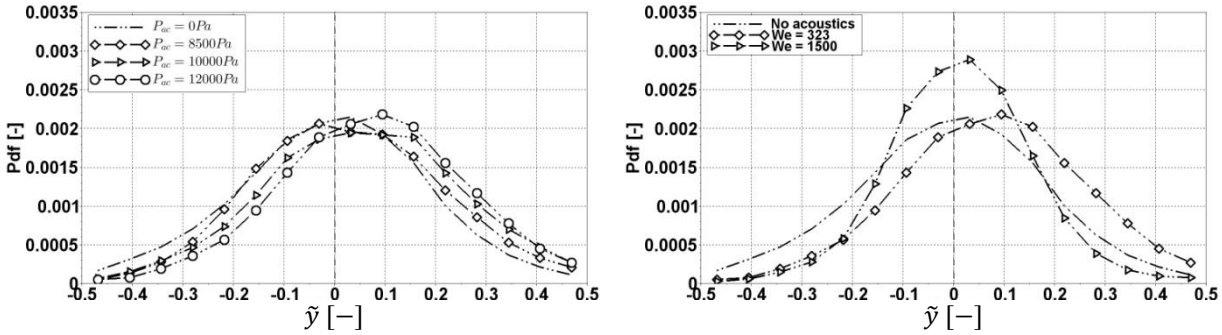

Figure 5 Pdf at IAN for the fiber regime as function of the acoustic level (left) and of the Weber number (right).

The effects the acoustic level on spray deviation is shown on the left side of Figure 5 for the case of fiber regime at IAN. The curve relative to P_{ac} = 12000 Pa is the one already discussed before. It is clear that decreasing the maximum intensity of the acoustic field the curve tends to be more and more symmetrical indicating that the deviation produced by the acoustics field is less pronounced.

The sensitivity of the spray deviation to the Weber number in fiber regime is shown on the right side of Figure 5. As Weber number increases, the effect of acoustics reduces and drop location Pdf tends to be more symmetrical around injection axis. This tends to confirm the competition between acoustics and aerodynamics effects on liquid drops in such conditions.

But, as acoustics can lead to the same final state independently from the initial one it can be inferred that producing an acoustic field with higher intensity than the one reachable in our experiment, the spray in fiber regimes should provide the same response whatever the Weber number.

Due to the size of the field of view some droplets are inevitably lost during acquisition. Such a loss is symmetrical at VAN and PAN, but not in all other cases (Figure 4b, c and d) where, due to the acoustic effects, the spray is deviated toward the right side of the image. In these three cases the distributions tend to zero on the left side of the image while a residual tail is observed on the right side of the plots.

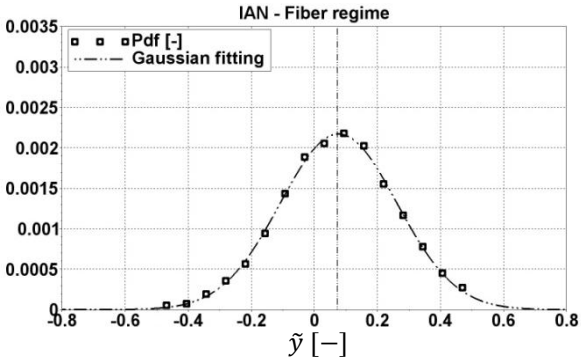

Figure 6 Example of Pdf fitting based on Gaussian function in the case of the fiber regime in correspondence of the intensity anti-node.

The more the deviation is pronounced the more objects are lost on the right side of the image, and less on the left side.

In order to quantify the spray deviation, a fitting of the probability distribution function based on a Gaussian function has been performed (see Figure 6). The mean value μ of the Gaussian is calculated and plotted in Figure 7 (adimensionalization by the width of the image has been performed). The more the droplets cluster is deviated, the larger is the value of μ. As shown in Figure 7, μ is lower in proximity of the pressure and velocity anti-node and is much bigger in all the three intermediate positions.

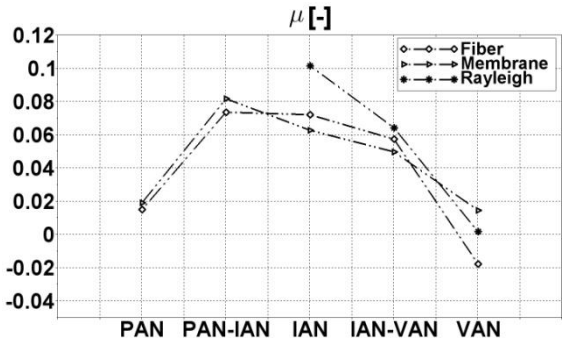

Figure 7 Mean value of the Gaussian fitting curve (left side). Right to left lost drops number ratio from provide by the Gaussian fitting function (right side).

In order to better quantify and distinguish the phenomenon of droplets production from the one of the deviation of droplets, a coefficient defined as $\beta = (N_{ac}-N_i)/(N_{ac}+N_i)$ has been introduced. Here N_{ac} is the number of drops during maximum acoustic amplitude, thus relative to the treatment of the sample indicated as ITac and N_i is the number of drops at the beginning of the test (ITi). If β is equal to 1 it means the droplets were not present without acoustics and are thus produced by the perturbation (N_i=0); If β is equal to 0 no modification in the droplets number is detected (N_{ac}=N_i) and if β is negative the number of droplets during acoustics is lower than the number of droplets without acoustics (N_{ac}<N_i).

Results relatives to the calculation of β are shown in Figure 8. In the case of the fiber regime (see left side of Figure 8) at VAN the coefficient is positive and ranges between 0.2 and 0.4 in the central part of the image ($-0.4 < \tilde{y} < 0.4$) indicating a large production of drops with respect to the initial spray configuration in the central part while tends to 0 on the sides where $N_i \sim N_{ac}$. In correspondence of the other three locations the coefficient is non-symmetrical respect to the central axis of the jet. On the left side of the image β is negative indicating that N_i>N_{ac}. This is due to the fact that fewer droplets are produced by acoustics respect to the VAN and moreover they are deviated to the right side of the image where the coefficient is positive as in the case of IAN-VAN and IAN, or close to 0 as in the case of PAN-IAN, indicating that there is no substantial variation in terms of drops number. For what concerns the membrane regime a relatively small quantity of droplets is present without acoustics and thus the coefficient β is always positive. It is included between 0.6 and 1 in the case of VAN and IAN-VAN, indicating a large production of drops. In particular β is close to 1 on the sides, where N_i/N_{ac} tends to 0 since almost no drops are present at the beginning, and it is in between 0.6 and 0.8 in the central part of the jet, where the big liquid blobs present without acoustics are broken by acoustics.

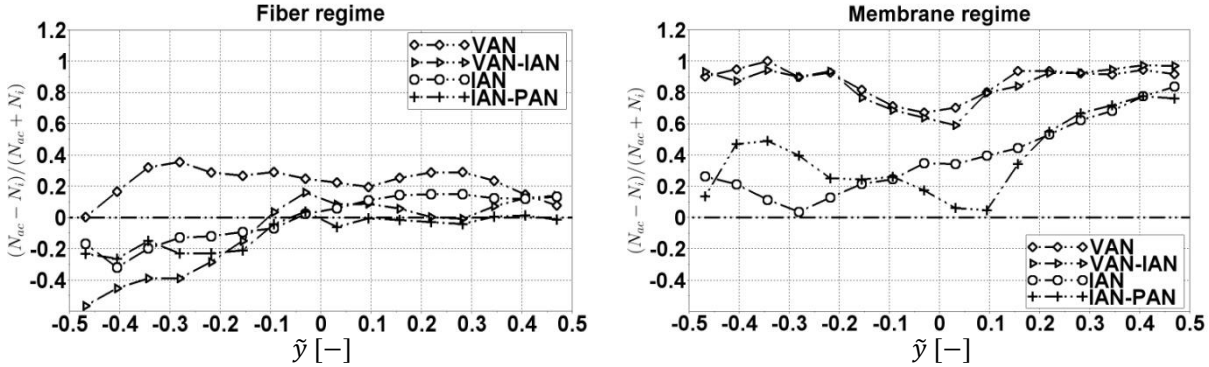

Figure 8 Horizontal spatial evolution of coefficient β for the fiber regime (left side) and for the membrane regime (right side).

In the other two cases, namely IAN and PAN-IAN, the coefficient β is still positive, but as already observed for the fiber regime it is not symmetric. In particular at IAN the coefficient has a minimum around $\tilde{y} = -0.3$ and grows up on the left side until 0.2 and until 0.8 on the right side. In the case of PAN-IAN the minimum is reached around $\tilde{y} = 0.1$, on the left side β grows up to 0.5 while on the right it reaches 0.8. In both cases β increases on the right side much more than the left one indicating that droplets produced are deviated on the right side of the image toward the velocity anti-node. The minimum represents the spatial class where the quantity of

elements coming from the nearest left class almost balances the number of elements that move away from the class toward the right side of the image.

Summary and Conclusions

The response of coaxial jets to a transverse acoustic field with maximum amplitude of 174 dB has been investigated. Several atomization regimes and locations with respect to the acoustic axis have been taken into account. The horizontal spatial probability density functions Pdf have been calculated and compared for different regimes at a fixed location, and for the fiber regime at IAN as function of P_{ac}. Results have shown that the Pdf calculated on image sequence extracted during acoustics in the case of the highest Weber number regime considered (fiber regime) presents the same trend of the Pdf calculated for all other regimes at lower Weber number, for all locations considered. Thus, it can be inferred that with a sufficiently high amplitude acoustic field even regimes at very high Weber and Reynolds numbers can be affected by acoustics and provide the same behaviour observed in the experiment discussed here.

In particular two different phenomena caused by acoustics have been observed for all regimes considered.

The first one is the intensification of the atomization process by rupture of big liquid blobs and drops into smaller ones. This process is mainly observed in correspondence of the velocity anti-node and decreases going toward the pressure anti-node where no effects are observed. At VAN, in fact, acoustic velocity is high enough to increase shear stress acting on jet and droplets accelerating the break-up process and subdivisions of largest droplets by secondary atomization.

The second phenomenon observed is the deviation of the spray similar to the flame deviation observed by Méry [3]. Deviation is observed at first in between the velocity anti-node and the intensity anti-node and shows his maximum in between the pressure anti-node and the intensity anti-node where the other phenomenon stops to show up. Droplets produced by atomization and/or by acoustics are deviated toward the nearest velocity anti-node causing a desertification around the pressure anti-node and a clustering around the velocity anti-node. Such a deviation can be explained by taking into account the radiation force.

In a liquid rocket combustion chamber where hundreds of injectors are present and pressure fluctuations can reach very high amplitude consequences can be dramatic. The main result is a non uniform redistribution of droplets with consequent spatial non-homogeneity of heat release. Droplets clustering in correspondence of the velocity anti-node can lead toward a velocity driven coupling mechanism as observed by Sliphorst et al. [2].

Moreover, acoustic mode enhancing atomization directly affects the combustion process, shortening the flame, augmenting the heat flux to the chamber walls and injection plane.

Acknowledgements

This study was granted by CNES R&D program, in the frame of the activity of French-German research group REST (Rocket Engine Stability Research Initiative).

References

[1] V. Yang, W. Anderson, Liquid rocket engine combustion instability, *Progress in Astronautics and Aeronautics*, **169**, (AIAA, Washington, DC, 1995).

[2] M. Sliphorst, B. Knapp, S. Gröning, M. Oschwald, Combustion instability coupling mechanism between acoustics and Lox/CH4 spray flames, Journal of Propulsion and Power, Vol.28, pp. 1339-1350, 2012.

[3] Y. Méry, Mécanismes d'instabilités de combustion haute-fréquence et application aux moteurs-fusées, PhD thesis, École Centrale Paris (2010).

[4] F. Baillot, J.B. Blaisot, G. Boisdron, C. Dumouchel, Behaviour of an air-assisted jet submitted to a transverse high frequency acoustic field. *J. Fluid Mech*., **640**, 307-344 (2009).

[5] F. Baillot, J.B. Blaisot, C. Richard, M. Théron, Effects of acoustic radiation on air-assisted jets in a transverse high-frequency acoustic field. In 25th European Conference on Liquid Atomization and Spray Systems (ILASS Europe), Chania, Greece (2013).

[6] G. Boisdron, Etude de l'atomisation d'un jet liquide assisté par air soumis á une onde acoustique stationnaire transverse haute fréquence, PhD thesis, University of Rouen (2006).

[7] J.C. Lasheras, E.J. Hopfinger, Liquid jet instability and atomisation in a coaxial gas stream. *Annu. Rev. Fluid Mech*., **32**, 275-308 (2000).

[8] N. Fdida, Développement d'un système de granulométrie par imagerie application aux sprays larges et hétérogènes, PhD thesis, University of Rouen (2008).

[9] L.V. King, On the acoustic radiation pressure on spheres. *Proc. R. Soc. Lond. A*, **147** (861), 212-240 (1934).

[10] A. P. Zhuk, Radiation force acting on a cylindrical particle in a sound field. *Prikl. Mekh*., **22**. No. 7, 103-108, (1986).